Corresponding Author: Dr. Philippe Buechler, PhD

Corresponding Author's Institution: University of Bern

First Author: Elena Businaro

Order of Authors: Elena Businaro; Harald Studer; Bojan Pajic; Philippe Buechler, PhD

Abstract: Image-based modeling is a popular approach to perform patient-specific biomechanical simulations. One constraint of this technique is that the shape of soft tissues acquired in-vivo is deformed by the physiological loads. Accurate simulations require determining the existing stress in the tissues or their stress-free configurations. This process is time consuming, which is a limitation to the dissemination of numerical planning solutions to clinical practice. In this study, we propose a method to determine the stress-free configuration of soft tissues using a Gaussian Process (GP) regression. The prediction relies on a database of pre-calculated results to enable real time predictions. The application of this technique to the human cornea showed a level of accuracy five to ten times higher than the accuracy of the topographic device used to obtain the patients' anatomy. In this context, we believe that GP models are suitable for predicting the stress free configuration of the cornea and can be used in planning tools based on patient-specific finite element simulations. Due to the high level of accuracy required in ophthalmology, this approach is likely to be appropriate for other applications requiring the definition of the relaxed shape of soft tissues.

- Gaussian Process (GP) regression was proposed to obtain the stress-free configuration of soft tissuesmeasured under physiological loads
- Application on the human cornea was based on more than 1000 datasets
- Determination of the stress-free configuration is instantaneous
- The stress-free configuration was at least five 5 times more accurate than the clinical requirements

1 # Gaussian process prediction of the stress-free

2 # configuration of pre-deformed soft tissues:

3 # Application to the human cornea

4 Elena Businaro[1,2], Harald Studer[2], Bojan Pajic[3,4,5,6]& Philippe Büchler[1]

5 [1]Institute for Surgical Technology & Biomechanics, University of Bern, Switzerland

6 [2]Integrated Scientific Services AG, Biel, Switzerland

7 [3]Swiss Eye Research Foundation, Eye Clinic ORASIS, Reinach AG, Switzerland

8 [4]Division of Ophthalmology, Department of Clinical Neurosciences, University Hospitals of

9 Geneva, Switzerland

10 [5]University of Novi Sad, Faculty of Sciences, Faculty of Physics, Novi Sad, Serbia

11 [6]Medical faculty, Military Medical Academy, University of Defense Belgrade, Serbia

12

13

14

15

16

17

18

19

20   Address for correspondence:

21   Philippe Büchler

22   Institute for Surgical Technology & Biomechanics

23   University of Bern

24   Stauffacherstrasse 78

25   3014 Bern, Switzerland

26   Phone: +41 31 631 5947

27   Email: philippe.buechler@istb.unibe.ch

28

29

Abstract

Image-based modeling is a popular approach to perform patient-specific biomechanical simulations. One constraint of this technique is that the shape of soft tissues acquired in-vivo isdeformed by thephysiologicalloads. Accurate simulations require determining the existing stress in the tissues or their stress-free configurations. This process is time consuming, which is a limitation to the dissemination of numerical planning solutions to clinical practice. In this study, we propose a method to determine the stress-free configuration of soft tissues using a Gaussian Process (GP) regression. The prediction relies on a database of pre-calculated results to enable real time predictions. The application of this technique to the human cornea showed a level of accuracyfive to ten times higher than the accuracy of the topographic device used to obtain the patients' anatomy. In this context, we believe that GP models are suitable for predicting the stress free configuration of the cornea and can be used in planning tools based on patient-specific finite element simulations. Due to the high level of accuracy required in ophthalmology, this approach is likely to be appropriate for other applicationsrequiring the definitionof the relaxed shape of soft tissues.

45

1 Introduction

The recent progress in medical image analysis and numerical simulation tools enabled thedevelopmentof patient-specific planning solutions based on biomechanical simulations. The anatomical information for each patient is derived from medical imaging and finite element simulations are used to evaluate the outcome of specific surgical interventions. Additionally, such simulationplatforms allow further understanding of the disease, its progression and on the efficacy of availabletreatments and procedures.

One of the problems with this approach is that the medical images acquired in-vivo describe the tissue in its physiological situation, which is frequently under stress. This is typically the case for soft tissue such as ligaments, arteries or the human eye. However, the level of initial strain in the tissue cannot be directly measured on the patient,therefore the biomechanical models are considering an initially unloaded "stress-free" configuration[1]. Several methods were proposed to pre-stress the measured 'initial' geometry[1-4]. Among these methods, some researchers proposed an inverse elastostatic approach centered on the reverse application of in-vivo conditions to explicitly estimate the stress-free configuration, hence one non-linear simulation step is required to update the deformation gradient tensor [5–7]. Others adopted a modified updated Lagrangian formulation [1,2,8], to estimate the stress in the tissue using a forward calculation, where the procedure continuously updates the deformation tensor during the simulation of the in-vivo state. Although these methods provided accurate results, they require complex implementations, and – especially when the tissue is considered incompressible –athorough knowledge of continuum mechanicsas well as the solution of a non-linear problem. By contrast, an easier approach has been proposed by Pandolfi [9], where a simple analytic calculation is combined with finite element analysis to obtain the stress-free configuration of the tissue. High accuracy can be achieved with this approach, but the solution requires the iterative solution of a finite element problem, which is time consuming[2,11,24].

Calculation time represents an important issue for the acceptability of the planning tool in clinical routine. Therefore, the stress-free configuration of the tissues should be obtained as efficiently as possible. For this reason, the aim of this study was to evaluate prediction of the relaxed shape of the tissue with a stochastic approach.The Gaussian process (GP) is one of the most widely used stochastic and non-parametric processes for modeling dependent data observed over space or time. It has been used for several biomechanical applications to predict human gait kinematics [15], abdominal aortic aneurysms [16] or for the estimation of swimming velocity [17]. Our hypothesis was that this method could also be suitable to estimate the patient-specific stress-free configuration starting from clinical images. In this work, the parameters describing the shape of the tissue were modeled as a Gaussian process, which was used to predict the stress-free configuration without any further finite-element analysis. The method has been applied in ophthalmology for the prediction of the relaxed shape of the cornea that will be used in a planning solution for refractive surgeries.

2   Material & Methods

In order to compute the stress free configuration of the cornea using aGaussian Processapproach, several steps were necessary. First,the corneal geometrical information was acquired with a topography device (Section 2.1); the geometrical information thus obtained was used to deform a spherical cornea template to create patient-specific finite element meshes(Section 2.2).Patient specific models were then pre-stressed with an iterative approach (Section2.3) and the resulting stressed corneas were divided into training and test data (Section 2.4.1). The training data was used to build the Gaussian process model (Section 2.4.2) and the test datawas used to assess the quality of the predictionobtained with the fitted Gaussian process model(Section 2.4.3).

2.1   Patient Data

Theshape of 1738 patients corneas were acquired with a Pentacam HR Scheimpflug camera.This topography device allows an accurate measurement of the anterior and

98   posterior surface of the cornea (accuracy of a few microns) and to export the geometric

99   measurements as Zernike[18] polynomials. The Zernike coefficients $W(r,\theta)$ describe the

100   elevation data of both the anterior and the posterior corneal surfaces. This decomposition is

101   frequently used to describe the shape of the corneal surface, because the Zernike

102   polynomials Z_n^m represent an orthonormal basis where each polynomial function describes a

103   distinct optical property of the refractive surface (i.e. defocus, astigmatism, coma, trefoil,

104   quadrafoil).Therefore, any points on the corneal surface can be defined in a polar coordinate

105   system r,θ as:

$$W(r,\theta) = \sum_{n=0}^{k} \sum_{M=-n}^{n} W_n^m Z_n^m (r,\theta)$$

106   where W_n^m are the Zernike coefficients defining the weights, n and m are respectively the

107   order and phase of the polynomial. Zernike polynomials up to order $k \leq 6$ have been

108   considered in this study.

2.2   Finite element model

110   Patient-specific models of the cornea where obtained by morphing a template finite element

111   mesh to the topographic measurements.The three-dimensional template mesh included both

112   the cornea and sclera(Figure 1), which were meshed with about 40000 linear hexahedral

113   elements [20]. A no-displacement boundary condition has been applied to the nodes located

114   on the cut-section through the sclera. A normal intraocular pressure of 15 mmHg has been

115   applied on the internal surface of the mesh.

116   A mechanical model previously published and validated has been used to describe the

117   mechanical behavior of the tissue[19,20].Briefly, the strain energy function of the constitutive

118   material model is given below:

$$\Psi = U + \bar{\Psi}_m + \frac{1}{\pi} \int \Phi(\theta) \cdot \left(\bar{\Psi}_{f1} + \bar{\Psi}_{f2} \right) d\theta$$

119   where U describes a penalty function to ensure incompressibility of the material, $\overline{\Psi}_m$ is a neo-

120   Hookean material representing the tissue matrix, $\overline{\Psi}_{f1}$ and $\overline{\Psi}_{f2}$ are modified Ogden materials

121   [21] modeling the main collagen fibers and the collagen cross-linking, respectively. The

122   probability distribution function Φ defines a realistic fiber distribution [22] by assigning

123   weights to each fiber direction. Material constants were determined using three sets of

124   experimental data obtained on button inflation tests [23] and strip extensiometry [14].

125   ## 2.3   Iterative Pre-Stressing Process

126   The in-vivo corneal shape measured by the Pentacam device was stressed by the

127   physiological intraocular pressure. An iterative approach was applied to progressively move

128   the nodes of the patient-specific finite element mesh toward their stress-free shape. In this

129   study the iterative approach, proposed by Elsheikh et al. [24] and Pandolfi et al. [9], was

130   used.

131   Assuming the coordinates of the patient-specific model (X_0) as the target of the iterative

132   process, x_i describes the corneal geometry after each iteration i resulting from the nodal

133   displacement induced by the intraocular pressure (IOP). The computed nodal displacements u_i

134   are then used to estimate the stress-free form X_i and the error e_i:

$$e_i = x_i - X_0 = (X_i + u_i) - X_0$$

$$X_{i+1} = X_0 - u_i$$

135   The root mean square distance was used to monitor the convergence of the iterative process

136   to the stress-free form. The iterative process was stopped when this error dropped below

137   10^{-4} μm, which usually requires about 10 iterations.

138   ## 2.4   Gaussian Process

139   A Gaussian process was defined to predict the stress-free configuration of the cornea. The

140   model parameters were fitted to generate a functional mapping between the shape of the

141   cornea measured experimentally and the corresponding stress-free configuration. In this

study, the Matlabimplementationof Gaussian Process for Machine Learning proposed by Rasmussen[25] has been used.

2.4.1 Training and Test Datasets

This dataset consists oftraining input vectorsx_s, containing the Zernike coefficients describing the shape of each patient's corneaunder stress,as well astraining output vectorsy_s, containingthe Zernike coefficients describing the stress-free shape of these corneas. The parameters of the output matrix y_s were obtained with the pre-stressing techniquedescribed previously.

The training dataset represents the pool of data that was used to determine the Gaussian Process. To evaluate the effect of the size of the training data on the predictions, several GP models were fitted on gradually increasing number of training data. Four GP models have been fitted to datasets containing 250, 500, 750 and 1663 corneas. In this evaluation the training dataset included of mix of healthy and pathological corneas, while the test dataset consisted of 75 healthy corneas.

Further GP models were built to verify the effect ofdiscriminating healthy from pathological corneas within the training dataset. For this evaluation,we used twotraining datasets,each containing 700 corneas from healthy and pathologicalpatients,respectively. Separate datasets containing respectively75 pathological and 73 healthycorneas were used to evaluate the quality of the predictions.

2.4.2 Design of Gaussian process model

A GP can be considered as a collection of random variables indexed by a continuous variable: $f(x)$.Suppose we define a particular finite subset of these random variables $f(x) = \{f_1, f_2, \ldots, f_N\}$, with corresponding inputs$x = \{x_1, x_2, \ldots, x_n\}$. In a GP, any such set of random function follow amultivariate Gaussian distribution, which means that every linear combination of its components $f = a_1 x_1 + a_2 x_2 + \cdots + a_n x_n$ is normally distributed for any

167   vector a $\in \mathcal{R}^k$.A Gaussian process follows a normal distribution and is therefore completely

168   defined by its mean and covariance functions [25]:

$$f(x) \sim \mathcal{N}\left(m(x), K(x, x')\right)$$

169   with mean $m(x)$ and covariance function $K(x, x')$. In this study, the mean function wasfixed

170   to zero($m(x) = 0$), which was not a strong limitation since the data can becentered in a pre-

171   processing step. A squared exponential covariance was used as covariance function:

$$K(x, x') = \sigma_f^2 e^{-\frac{(x-x')^2}{2l^2}}$$

172   where$l$is the characteristic length-scale and σ_f^2controls the overall variance of the process.

173   In realistic modeling situations, only noisy data are availableof the output function

174   values.Therefore a Gaussian noise ε was added to the data such as:$y = f(x) + \varepsilon$,having a

175   zero meanand a variance σ_n^2.The parameters l, σ_f^2 and σ_n^2correspond to the

176   hyperparameterθcharacterizing the GP model.Thehyperparametersthat best represent all

177   data in the training set are obtained by maximizing the Gaussian likelihood amongst the

178   training dataset:

$$\log p(y|X, \theta) = -\frac{1}{2} y^T C^{-1} y - \frac{1}{2} \log|C| - \frac{n}{2} \log 2\pi$$

179   where $C = K(x, x') + \sigma_n^2 I$ is the covariance function for the noisy targets$y$. The first term can

180   be interpreted as a data-fit term, the secondterm is a complexity penalty and the last term is

181   a normalizing constant.

182   2.4.3   Gaussian Process Prediction

183   In order to make predictions,the Zernike coefficients estimated for the test dataset were

184   compared with the stress-free shape resulting from the iterative process. The prediction $y_{tp\,m}$

185   of the mth Zernike coefficient defined in the output of test dataset $y_t$is obtained as:

$$mean\left(y_{tp\,m}\right) = K(x_t, x_s)[K(x_s, x_s) + \sigma_n^2 I]^{-1} y_{s^m} = K(x_t, x_s)\alpha_m$$

$$cov(y_{tp\,m}) = K(x_t, x_t) - K(x_t, x_s)[K(x_s, x_s) + \sigma_n^2 I]^{-1} K(x_s, x_t)$$

186 where K is the covariance function, x_s and x_t are the training and the test input

187 respectively,and y_{s^m} is theoutput of the training data.The first formula establishes that alinear

188 predictor of the test output $y_{tp\,m}$ obtainedby multiplication of the covariance between training

189 and test input by a pre-computed vector α_m, which only depends on training data.

190 Several optical parameters have been used to quantify the error of the GP predictions. These

191 parameters included the keratometricindices, average curvature indices and wavefront

192 aberration parameters. Keratometricindices are based on the average curvature of the

193 steepest (SimKs) and flattest (SimKf) meridian on the corneal surface (given in diopters).

194 They are calculated over a central corneal annulus of 0.5 to 2.5mm radius. The keratometric

195 indices are the induced cylinder (SimKs – SimKf) and the induced change in average K

196 (SimKs+SimKf)/2.0. Averaged axial curvature indices describe corneal shape in three

197 important regions; the central, paracentral, and peripheral zones. Central average curvature

198 is calculated over the central annulus of 0.0 to 2.0mm radius, the paracentral average

199 curvature is calculated over an annulus of 2.0 to 3.5mm radius and the peripheral average

200 curvature is calculated over an annulus of 3.5 to 5.0mm radius.Wavefront aberration is

201 calculated from surfaces andis described by the following indices given as the average of the

202 coefficients obtained by Zernike decomposition of the anterior cornea; the spherical

203 aberration(Z_4^0), coma $(Z_3^{-1} + Z_3^1)/2$, trefoil $(Z_3^{-3} + Z_3^3)/2$, tetrafoil($Z_4^{-4} + Z_4^4$)/2and the root

204 mean square (RMS) of the aberrations of order 4 and higher ($>Z_3^x$).

3   Results

206 The Gaussian process has been run to predict each Zernike coefficient required for the

207 description of the anterior and posterior surfaces of every patients' stress-free shapes. The

208 output of the GP includes the mean of the predicted variable as well as the variance

209 associated with this parameter (Figure2).

210 Four GP models have been created by gradually increasing the number of training data
211 respectively 250, 500, 750, 1663. For a quantitative analysis, optical indices describing the
212 stress-free shape have been considered. Differences calculated between the optical indices
213 of the stress-free shape obtained with the pre-stressing iterative approach and the optical
214 indices of the stress-free shape predicted with the GP modelshowed that for almost all
215 optical indices, the curvature error did not exceed 0.025 D, while the wavefront aberration
216 percentage error did not overcome 5%. This limit has been chosen because 0.025D is ten
217 times smaller than an optical error perceptible by the patient. Moreover, results showed that
218 the mean error was always around zero while the standard deviation of the error decreased
219 with increasing size of the training data, reaching a plateau at about 1000 Training Data
220 (Figure 3).Additionally, the corneal surface predicted using the GP model were analyzed.The
221 Instantaneous Curvature maps of the stress-free shape, obtained with the pre-stressing
222 iterative approach were compared to the maps obtained using the Zernike coefficients
223 predicted bythe Gaussian Model.The maps produced using the prediction model were
224 qualitatively identical to the target corneal shape (Figure 4).

225 TwoGP models were calculated to determine if separating healthy from pathological corneas
226 in the training dataset could improve the predictions. For all the optical parameters, the mean
227 error was always around zero. Results indicated that the training dataset including only
228 healthy cornea provide slightly better predictions for healthy cornea than pathological ones.
229 The opposite was also true; the pathological training dataset provide a better estimation of
230 the stress-free shape of pathological corneas than of healthy ones (Table 1). However, the
231 difference observed on the optical parameters remained small, which indicates that the
232 model based on pathological training data is not able to significantly improve the
233 predictionsin pathological situations. In addition, with the model built on healthy corneas,
234 95% of the predictions remain within the boundaries of the targeted accuracy.

235 The predicted stress-free configurations were then used to calculate the shape of the cornea
236 after physiological loading.The comparison of the stressed shape with the target topographic

237 measurements acquired on the patients, showed that thecurvature mean error differs from

238 zero in almost all cases, indeedmost GP predictions lead to curvature errors exceeding

239 therange of 0.025D (Table 2). Inthe worst case, the error could reach 0.05 D when theGP

240 model wascreated by considering only pathological corneas.Besides,it seems that GP

241 induced a slight underestimation of the central average curvature and a small overestimation

242 of the peripheral average curvature in all cases. Overall, the results of the stressed shape

243 showed that 80% of the patients had small predictionerrors(<0.025D and <5%) on all the

244 shape parameters simultaneously and 93% of the patients in the test group had all the shape

245 parameters below the accuracy acceptableclinically (<0.05D and<10%).

246 ## 4   Discussion

247 Recently, numerical models have also been proposed as tools to better understand the effect

248 of surgeries on the eye, to support surgical intervention and to predict the refractive outcome

249 [9, 10]. To reach these goals, mechanical properties of cornea and sclera have been

250 characterized [11,12,13,14] and an accurate description of the shape of the patients' corneas

251 has been provided by ophthalmological measurement devices. Since the measured shape is

252 under tension due to the intra-ocular eye pressure, this information cannot be directly used to

253 perform patient-specific simulation; hence a pre-stressing approach is necessary. Simulation

254 time is always a critical point for clinical application. Therefore, the pre-stressing calculation

255 phase represents a strong limitation to the dissemination of biomechanical planning to

256 clinical applications. A non-parametric approach has been used to predict the stress-free

257 configuration of the cornea in real time.

258 The results obtained with this method showed that the prediction accuracy could reach a

259 level suitable for a clinical application. The current topographic devices used to measure the

260 shape of the cornea reach an accuracy of $\pm$0.25 D. In this work, we aimed at reaching an

261 accuracy of 0.025 D for corneal shape stresses by the IOP, which is 10 times better than the

262 accuracy of the input data.Results showed that for a GP model fitted on healthy data, the

263 target accuracy has been achieved for most of the optical parameters, but the prediction

264 accuracy always remained below 0.05 D, which is 5 times better than the accuracy provided

265 by the input devices. Considering that curvature information is challenging to predict, the

266 level of accuracy reached with the proposed approach is high and seems appropriate for

267 surgical planning. In all cases, accuracy of the predictions was largely superior tothe

268 precision of modern topography devices.

269 Different prediction models can be used according to the patient demographic information

270 such as age, sex or specific pathology. In this study, a rough separation of the data has been

271 performed between healthy and pathological. The results indicated that models solely based

272 on pathological datasets were not able to better predict the stress-free configuration of the

273 pathological data. A possible explanation is that many different ophthalmic diseases were

274 combined inside this pathological group, but with a small number of instances for each of the

275 pathologies. There are many different corneal changes induced by pathology; for example a

276 keratoconus shows completely different corneal shapes than a Fuchs-Endotheldystrophy. It

277 is also clinically known that Laser-Assisted in situ Keratomileusis(LASIK)treated by tissue

278 saving algorithms induces a spherical aberration. Due to the amount of patient information

279 available, it was not possible to refine the analysis and propose disease-specific models, but

280 we believe that such models would further improve the prediction accuracy.

281 Under physiological loading, the stress-free configuration should match the shape of the

282 Pentacam data acquired on the patients. Our calculations indicate that the minor deviations

283 observed on the stress-free configuration were amplified by the application of the internal

284 ocular pressure. However, the results achieved with this method remain close to the target

285 accuracy for 95% of the samples. In addition, all the optical parameters have a mean

286 prediction very close to the experimental data, but the standard deviation of the prediction

287 error increased during pre-stressing. Again, when the GP model is built on healthy data,

288 results showed that the predictions are acceptable for clinical applications and that the

289   accuracy of the reconstructed shape remains at least five times better than the accuracy of
290   current topographic tools.

291   The GP process proved to be an efficient technique to quickly predict the stress-free shape
292   of the cornea. However, the method relies on a large database of pre-calculated results. This
293   means that computational resources required to run the finite element simulations was not
294   suppressed, but shifted in a pre-processing step. Despite the burden to run a large number
295   of FE simulations, this approach has some benefits. The calculations are performed offline
296   and can be verified by simulation experts avoiding any potential problem with model
297   configuration, simulation convergence or other simulation errors. Dedicated hardware can be
298   used for this purpose and the nature of the problem makes it easily parallelizable. As a
299   consequence, a verified model can be delivered to the clinician. In addition, a relatively low
300   number of input data was required to establish accurate prediction models. Results indicated
301   that 1000 patient datasets were sufficient to reach a plateau in the prediction accuracy.

302   The proposed method relies on the Zernike coefficient for the prediction of the shape, which
303   differs from the other pre-stressing approaches that rely on a finite element mesh. One of the
304   benefits of the Zernike coefficient is that it is a direct representation of the refractive surface.
305   The same approach based on finite element meshes would introduce inaccuracies from the
306   discretization and from the mapping of the nodes on the surface. The establishment of
307   correspondence on the corneal surface is difficult due to the lack of obvious landmarks. In
308   addition, the Zernike coefficients enable an arbitrary meshing of the stress-free configuration,
309   including eventual cut representing the surgical intervention.

310   The GP predictions proposed in this study are fitted to numerical simulations, which were
311   performed with a precise set of material parameters, boundary conditions and loads.
312   Although the finite element mesh selected doesn't affect the predictive model, alteration of
313   any other parameter defining the finite element model implies rebuilding the complete model.
314   This means that any improvement of the numerical model leads to heavy calculations since it
315   requires re-establishing the database of pre-calculated results. This limitation is mitigated by

316   the facts that the process can be mostly automated, that a relatively small number of input

317   models is required and that proper validation of the initial finite element model should be

318   performed before building this database.

319   The application of the GP modelshas been limited to the prediction of the stress free shape

320   of the cornea, because this corresponds to the most time consuming part of the overall

321   planning procedure. However, the proposed technique can be extended to include more

322   parameters representing the surgical intervention. Many refractive surgeries can be

323   described with a small number of parameters describing the length, depth and position of the

324   cut on the cornea. Of course, including the planning parameters in the predictive model is

325   expected to significantly increase the size of the training data. On the other hand, such

326   predictive model will provide the surgeon with real time prediction of the refractive outcome

327   and opens the door to truly optimize the surgical parameters.

328   Ophthalmology is very demanding in terms of accuracy, where surface topology is measured

329   in microns and curvature changes of a fraction of a diopter affect the patient's vision. In

330   addition, existing tools are available to quantify the shape of the tissue as part of clinical

331   routine, which enables the collection of a database of patient data to build and validate

332   prediction models. For these reasons, ophthalmology represents an ideal application for new

333   techniques aiming at predicting the stress shape of soft tissues. Based on the prediction

334   accuracy obtained on the stress-free prediction of the cornea, we conclude that this

335   technique is suitable as a first step of refractive planning solution. In addition, the same

336   approach could be used to predict the internal stresses of other soft tissue such as arteries

337   or ligaments.

5   Acknowledgements and declarations

6   References

347 [1] Gee, M.W., Förster, C., Wall, W.A., 2010. A computational strategy for prestressing

348 patient-specific biomechanical problems under finite deformation. International Journal for

349 Numerical Methods in Biomedical Engineering 26, (1):52–72.

350 [2] Grytz, R., Downs, J.C., 2012. A forward incremental prestressing method with application

351 to inverse parameter estimations and eye-specific simulations of posterior scleral

352 shells.Computer Methods in Biomechanics and Biomedical Engineering.

353 [3] Bols, J., Degroote, J., Trachet, B., Verhegghe, B., Segers, P., Vierendeels, J., 2013. A

354 computational method to assess the in vivo stresses and the unloaded configuration of

355 patient-specific blood vessels.Journal of Computational andApplied Mathematics 246, 10-17.

356

357 [4] Hsu, M.-C., Bazilevs Y., 2011. Blood vessel tissue prestress modeling for vascular fluid–

358 structure interaction simulation. Finite Elements in Analysis and Design 47, 593–599.

359 [5] Govindjee, S., Mihalic, P.A., 1998. Computational methods for inverse deformations in

360 quasi-incompressible finite elasticity. Journal for Numerical Methods in Biomedical

361 Engineering 43, (5):821–38.

362 [6] Govindjee, S., Mihalic, P.A., 1996. Computational methods for inverse finite elastostatics.

363 Computer Methods in Applied Mechanics and Engineering 136, (1–2):47–57.

364 [7] Lu, J., Zhou, X., Raghavan, M.L., 2007. Inverse elastostatic stress analysis in pre-

365 deformed biological structures: demonstration using abdominal aortic aneurysms. Journal of

366 Biomechanics 40, (3):693–6

367   [8] Lanchares, E., Calvo, B., Cristóbal, J.A., Doblaré, M., 2008. Finite element simulation of

368   arcuates for astigmatism correction. Journal of Biomechanics 41, (4):797–805.

369   [9] Pandolfi, A., Holzapfel, G.A., 2008. Three-dimensional modeling and computational

370   analysis of the human cornea considering distributed collagen fibril orientations. Journal of

371   Biomechanical Engineering 130, (6):061006.

372   [10] Roy, A.S., Dupps, W.J., 2011. Patient-specific modeling of corneal refractive surgery

373   outcomes and inverse estimation of elastic property changes. Journal of Biomechanical

374   Engineering 133, (1):011002.

375   [11] Pandolfi, A., Fotia, G., Manganiello, F., 2009. Finite element simulations of laser

376   refractive corneal surgery.Engineering with Computers 25, 15–24.

377   [12] Elsheikh, A., Geraghty, B., Rama, P., Campanelli, M., Meek, K.M.,

378   2010.Characterization of age-related variation in corneal biomechanical properties. Journal

379   of Royal Society Interface 7, 1475–85.

380   [13] Elsheikh, A., Geraghty, B., Alhasso, D., Knappett, J., Campanelli, M., Rama, P.,

381   2010.Regional variation in the biomechanical properties of the human sclera.Experimental

382   Eye Research 90, 624–33.

383   [14] Elsheikh, A., Brown, M., Alhasso, D., Rama, P., Campanelli, M., Garway- Heath, D.,

384   2008. Experimental assessment of corneal anisotropy. Journal of Refractive Surgery 24,

385   (2):178–87.

386   [15] Yun , Y., Kim, H., Shin, S. Y., Lee, J., Deshpande, A. D. , Kim, C., 2014. Statistical

387   method for prediction of gait kinematics with Gaussian process regression. Journal of

388   Biomechanics 47, 186-192.

389   [16] Ijaz, A., Choi, J., Lee, W., Baek, S., 2013. Prediction of Abdominal Aortic Aneurysms

390   Using Sparse Gaussian Process Regression.ASME Summer Bioengineering Conference,

391   SBC 2013.2013; 1B.

392 [17] Dadashi,F., Millet, G.P., Aminiam, K., 2013. Gaussian process framework for pervasive

393 estimation of swimming velocity with body-worn IMU.Electronics Letters- IEE 49(1). 44-46.

394 [18]Zernike, F., (1934). "Beugungstheorie des Schneidenverfahrens und Seiner

395 Verbesserten Form, der Phasenkontrastmethode". Physica 1, (8): 689–704.

396 [19] Studer, H., Larrea, X., Riedwyl, H., Buchler, P., 2010. Biomechanical model of human

397 cornea based on stromal microstructure. Journal of Biomechanics 43, 836–842.

398 [20] Studer, H. P., Riedwyl, H., Amstutz, C. A., Hanson, J. V. M., Buchler, P. 2013. Patient-

399 specific finite-element simulation of the human cornea: A clinical validation study on cataract

400 surgery. Journal of Biomechanics 46, 751–758.

401 [21] Markert, B., Ehlers, W., Karajan, N., 2005. A general poly convex strain-energy function

402 for fiber-reinforced materials. Proceedings in Applied Mathematics and Mechanics 5, 245.

403 [22] Aghamohammadzadeh, H., Newton, R., Meek, K., 2004. X-ray scattering used to map

404 the preferred collagen orientation in the human cornea and limbus. Structure 12, 249–256.

405 [23] Elsheikh, A., Wang, D., Brown, M., Rama, P., Campanelli, M., Pye, D., 2007.

406 Assessment of corneal biomechanical properties and their variation with age. Current Eye

407 Research 32, 11–19.

408 [24] Elsheikh, A., Whitford, C., Hamarashid, R., Kassem, W., Joda, A., Büchler, P., (2012).

409 Stress free configuration of the human eye. Medical Engineering and Physics 35, 211– 216.

410 [25]Rasmussen, C.E., 2006. Gaussian Processes for Machine Learning.
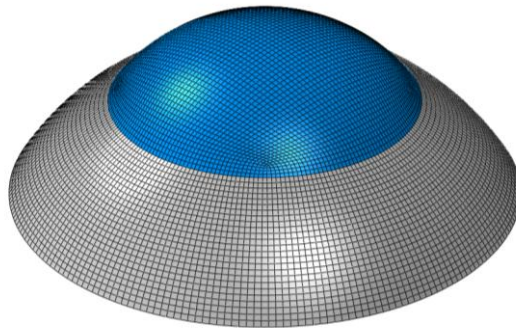
411

412

413

Figure1: Spherical finite element mesh of the cornea, which was used as a template to mesh the patients' anatomy obtained in-vivo. The blue and the gray parts represent the cornea and the sclerarespectively.
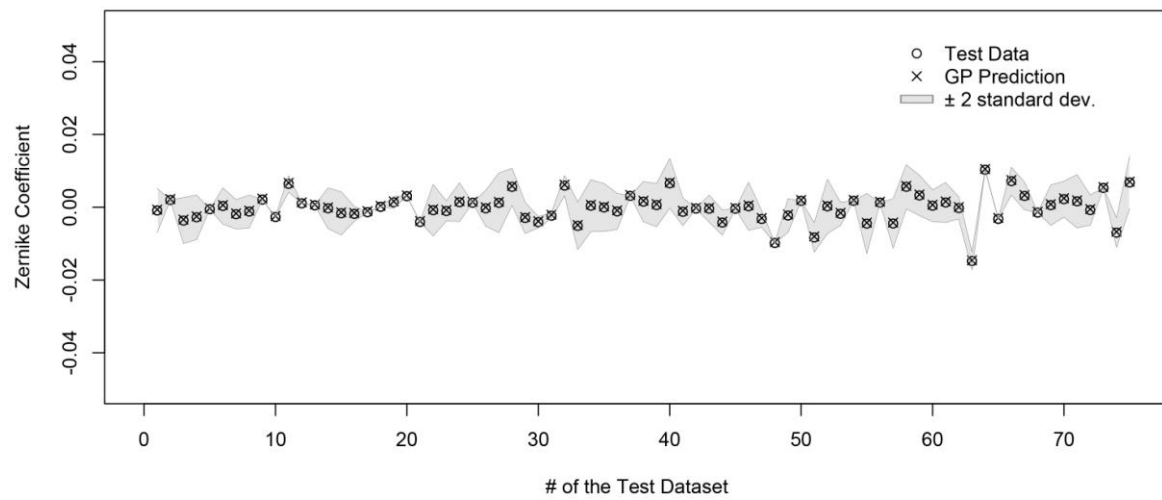
414

415

Figure 2: A Gaussian Model has been created with 250 Training Data. The graphs represent the results of prediction for one Zernike coefficient for each of the of 75 test data. The circles indicate the test data while the crosses are the GP prediction. The gray area representstwo standard deviationsas estimated by the GP predictions.
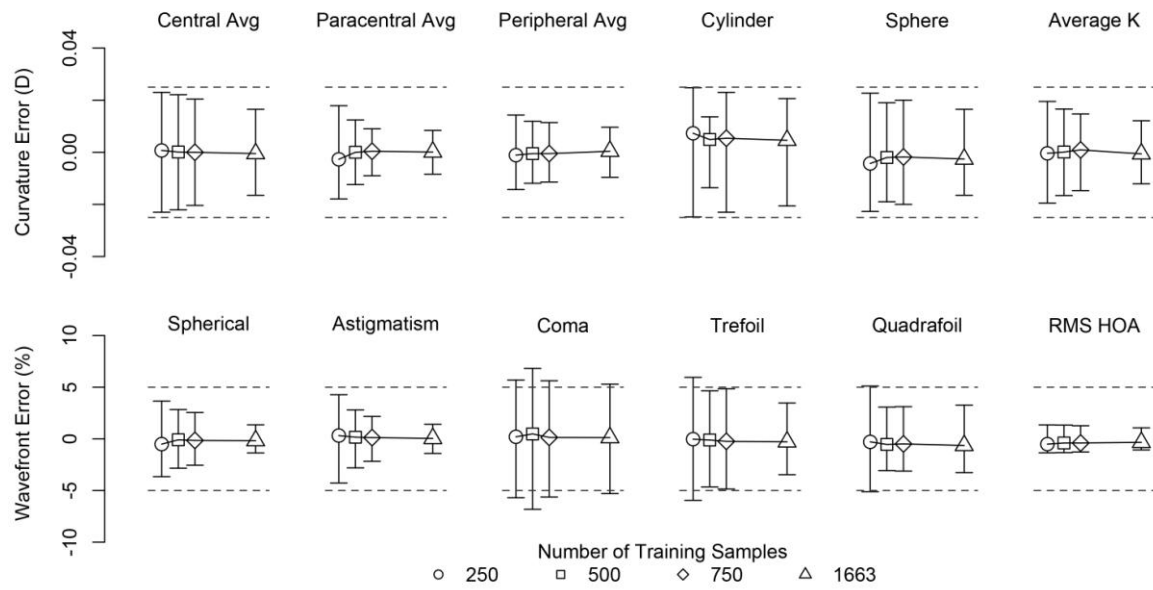
416

Figure 3: Accuracy of the GP prediction on the optical parameters of the cornea. The absolute mean error has been calculated in diopter (top)and the mean error on the wavefront aberration has been reported in percent (bottom). For each optical parameter, the accuracy of the prediction was reported for different size of the training data (250, 500, 750 and 1663). The error bars represented the variability of the data in a confidence interval of 95%. For most of the cases, the prediction error remains below the limits acceptable for clinical applications indicated by the dashed lines.
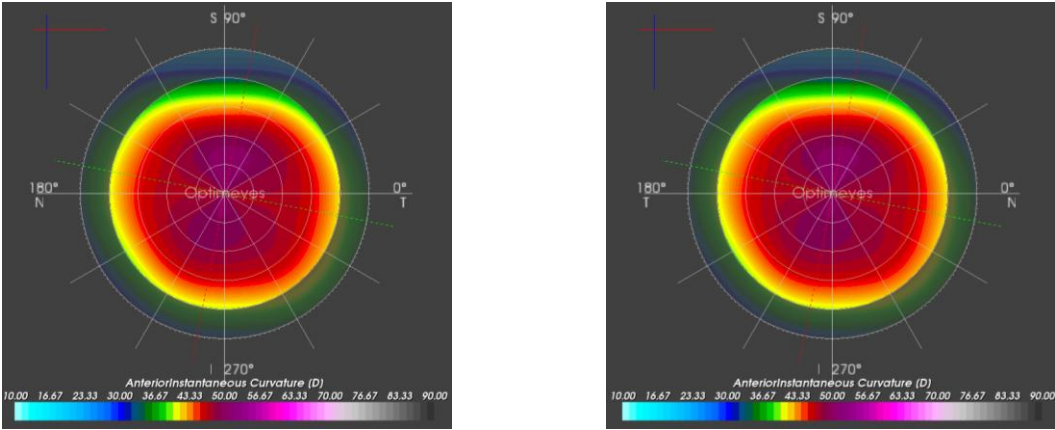
417

418

419

420

Figure 4: Instantaneous curvature obtained for the stress-free configuration obtained using the pre-stressing process (left) and predicted by the Gaussian model (right) for one of the reconstructed instance.

421

Stress Free Configuration		Healthy Training (700 datasets)		Pathological Training (700 datasets)	
		Healthy Test (72 Dataset)	Pathological Test (71 datasets)	Healthy Test (72 Dataset)	Pathological Test (71 datasets)
Curvature (D)	Average K	-0.0008 ± 0.0136	0.0015 ± 0.0247	-0.0006 ± 0.0155	-0.0005 ± 0.0178
	Cylinder	0.0061 ± 0.0245	0.0091 ± 0.0294	0.0059 ± 0.0220	0.0057 ± 0.0165
	Central Avg	-0.0010 ± 0.0184	0.0038 ± 0.0399	-0.0007 ± 0.0194	0.0004 ± 0.0215
	ParacentralAvg	-0.0013 ± 0.0111	-0.0003 ± 0.0101	-0.0008 ± 0.0145	-0.0004 ± 0.0164
	Peripheral Avg	-0.0010 ± 0.0107	0.0008 ± 0.0100	-0.0024 ± 0.0200	-0.0001 ± 0.0145
Wavefront aberration (%)	Spherical	-0.21% ± 2.38%	-0.30% ± 3.53%	-0.11% ± 2.63%	-0.30% ± 1.79%
	Astigmatism	0.06% ± 2.26%	-0.07% 1.66%	0.17% ± 2.98%	0.10% ± 1.75%
	Coma	0.14% ± 6.26%	-0.47% ±3.77%	0.25% ± 5.20%	-0.26% ± 3.63%
	Trefoil	-0.24% ± 4.34%	-0.07% ± 4.26%	0.03% ± 5.12%	-0.05% ± 5.28%
	Quadrafoil	-0.51% ± 3.54%	0.10% ± 7.76%	-0.49% ± 3.51%	0.20% ± 7.43%
	RMS HOA	-0.33% ± 1.09%	-0.21% ± 1.83%	-0.42% ± 1.17%	-0.32% ± 1.13%

Table1: Prediction error for the stress-free configurations calculated based on the GP. The error is indicated in diopters for the curvature parameters and in percent for the error on thewavefront aberration. The color code indicates the suitability of the predictions for clinical applications; green shows small prediction errors (<0.025D or <5%), yellow moderate prediction errors (0.025 – 0.05D or 5 – 10%). The average values is shown as well the 95% confidence interval (i.e. two standard deviations).

Stressed Configuration		Healthy Training (700 datasets)		Pathological Training (700 datasets)	
		Healthy Test (72 Dataset)	Pathological Test (71 datasets)	Healthy Test (72 Dataset)	Pathological Test (71 datasets)
Curvature (D)	Average K	-0.0065 ±0.0129	-0.0039 ± 0.0253	-0.066 ± 0.0151	-0.0050 ± 0.0165
	Cylinder	0.0050 ± 0.0153	0.0092 ± 0.0400	0.0066 ± 0.0204	0.0099± 0.0433
	Central Avg	-0.0081 ± 0.0192	-0.0046 ± 0.0379	-0.0083± 0.0190	-0.0066 ± 0.0194
	ParacentralAvg	-0.0011 ± 0.0124	-0.0007± 0.0109	-0.0008 ± 0.0153	-0.0010 ± 0.0155
	Peripheral Avg	0.0139 ± 0.0132	0.0139 ± 0.0133	0.0128 ± 0.0169	0.0130 ± 0.0145
WavefrontAberration (%)	Spherical	0.73% ± 2.78%	0.55% ± 3.37%	0.86% ± 3.56%	0.53% ± 1.56%
	Astigmatism	0.04% ± 3.57%	0.15% ± 3.59%	0.08% ± 4.77%	0.20% ± 3.62%
	Coma	0.08% ± 4.66%	0.08% ± 3.26%	0.05% ± 7.17%	0.23% ± 2.67%
	Trefoil	-0.12% ± 4.36%	0.55% ± 5.19%	0.06% ± 3.89%	0.52% ± 4.39%
	Quadrafoil	0.19% ± 2.44%	-0.16% ± 2.67%	0.39% ±2.76%	0.06% ± 2.67%
	RMS HOA	0.61% ± 0.86%	0.57% ± 1.41%	0.53% ± 0.92%	0.48% ± 0.89%

Table2: Prediction error for the stressed shape of the cornea obtained by simulating the internal ocular pressure on the stress-free configuration. The values reported in the table correspond to the difference between the prediction of the stressed shape using finite element simulation and the original topographic measurements. The error is indicated in diopters for the curvature parameters and in percent for the wavefront aberration errors. The color code indicates the suitability of the predictions for clinical applications; green shows small prediction errors (<0.025D or <5%), yellow moderate prediction errors (0.025 – 0.05D or 5 – 10%) and red shows prediction error that are considered as too large to ensure reliable surgical planning (>0.05D or >10%). For each parameter, the value represents the mean as well the 95% confidence interval (i.e. two standard deviations).

424

425